PERGAMON

International Journal of Heat and Mass Transfer 45 (2002) 3397–3404

International Journal of HEAT and MASS TRANSFER

www.elsevier.com/locate/ijhmt

Microscopic phenomena and macroscopic evaluation of heat transfer from plate fins/circular tube assembly using naphthalene sublimation technique

Jin-Yoon Kim, Tae-Ho Song *

Department of Mechanical Engineering, Korea Advanced Institute of Science and Technology, Kusong-dong 373-1, Yusong-gu, Taejon, South Korea

Received 25 July 2001; received in revised form 21 December 2001

Abstract

Flow and heat transfer in a plate fins/circular tube assembly is examined using naphthalene sublimation technique. The examined parameters are the gap (δ) to tube diameter (D) ratio δ/D, the Reynolds number Re_D and the tube location l/D for a single tube.

A preliminary flow visualization shows large recirculating twin vortices and a weak downstream oscillatory streakline. The local heat/mass transfer coefficient is large at the leading edge of the plate and also in front of the tube. It is relatively small behind the tube and it approaches the fully developed asymptotic value far downstream. The high heat/mass transfer coefficient in front of the tube is considered to be due to the so-called horseshoe vortex. When the Reynolds number is as large as 2660, a smaller subsidiary horseshoe vortex is attached to the upstream of the main one. The positive effect of the horseshoe vortices is prominent when the tube is placed in the downstream region. In this case, the total heat/mass transfer rate increases up to 25%.

1. Introduction

Plate fins/circular tube assembly is used in a wide variety of thermal engineering applications, for example, in air conditioning units, process gas heaters and coolers, compressor inter- and after-coolers, etc. Because of its wide use and simple geometry, many research groups have examined the performance.

Saboya and Sparrow [1,2] use the naphthalene mass transfer method to measure the local coefficients for one-row and two-row plate-fin and tube heat exchangers for $\delta/D = 0.193$. They report that the transfer rate is high on the forward part of the fins due to developing boundary layers as well as in front of the tube due to a vortex system there. However, no extensive search for optimal tube location is made. Jang et al. [3] compare the staggered arrangement of tubes with aligned one using experimental and numerical methods. Their study shows that the staggered arrangement gives greater heat transfer rate at the expense of increased pressure drop. Tsai and Sheu [4] study the complicated vortex systems in a two-row fin tube heat exchanger by using a three-dimensional numerical code. They give a highly detailed view of the physical processes. Onishi et al. [5,6] compute numerically a three-dimensional steady flow and conjugate heat transfer for one-row and two-row plate-fin tube heat exchangers. They report the effect of fin spacing, fin thickness, fin length, tube spacing and tube arrangement and the heat transfer performance though not completely extensive. Romero-Mendez et al. [7] study the effect of fin spacing over the overall heat transfer rate using flow visualization and numerical analysis, and report that the heat transfer can be increased by the increase of fin spacing at a fixed fluid velocity.

Until now, however, only minor attention is paid on the optimal configuration of the fin/tube assembly. To find out the optimal tube location, for instance, is as much important as to examine the microscopic thermophysical processes. In the present research, flow and heat transfer

* Corresponding author. Tel.: +82-428-693-032; fax: +82-428-693-210.

E-mail address: thsong@cais.kaist.ac.kr (T.-H. Song).

0017-9310/02/$ - see front matter
PII: S0017-9310(02)00047-9

Nomenclature

D	disk diameter
D_N	diffusion coefficient of naphthalene vapor in air
f	friction factor ($\equiv 2\Delta p\delta/\rho_{air}V^2L$)
h_m	mass transfer coefficient
k	thermal conductivity
L	length of test section
l	x-coordinates of disk center location
$\dot{m}''$	sublimation mass flux
$\dot{M}$	total mass flow rate of sublimated naphthalene
$\dot{Q}$	volume flow rate of air
Re_D	the Reynolds number ($\equiv UD/v$)
Sh_D	the Sherwood number ($\equiv h_mD/D_N$)
U	bulk velocity of air
W	span of test section
x	coordinates along the airflow
y	coordinates transverse to the airflow
z	vertical coordinates

Greek symbols

δ	gap size between two plates
τ	naphthalene sublimation depth
υ	kinematic viscosity of air
ρ_{air}	density of air
ρ_s	density of solid naphthalene
ρ_{sat}	saturation density of naphthalene vapor
ρ_{bulk}	bulk density of naphthalene vapor

in a plate fins/circular tube assembly is examined using the naphthalene sublimation technique. It is intended to scrutinize the microscopic flow and heat transfer phenomena and also to evaluate the overall performance to find out the optimal tube location.

2. Preliminary flow visualization

To find the overall flow field around the circular tube between two parallel plates, flow visualization is made using water. The plates are simulated by two glass plates. One glass plate is clear for observation and the other is backed with black paper to contrast with the white milk injected in front of the tube. The milk line reveals the streaklines. Two gap (δ) to tube diameter (D) ratios are arbitrarily tried, i.e., 0.06 and 0.11.

When the Reynolds number based on D is less than about 200, no appreciable wake behind the tube is observed for both of the δ/D ratios (see Fig. 1(a)). As the Reynolds number is increased, a pair of twin vortices appears behind the tube (see Fig. 1(b)).

When it is further increased (see Fig. 1(c)), the size of the twin vortices increases up to the tube diameter and the trailing streakline begins to oscillate. The Reynolds number at which this oscillation begins depends heavily on δ/D, i.e., it is about 1000 when $\delta/D = 0.06$ and 600 when $\delta/D = 0.11$. Note that Romero-Mendez et al. [7] report further evolution of twin vortices into oscillatory alternating vortices when $Re_D = 420$ and $\delta/D = 0.265$. It is obvious that the parallel plates suppress instability of the flow so that the evolution is suspended to greater Re_D when δ/D becomes smaller.

It is of interest that, for typical configurations in practical fin/tube assemblies, the flow field is neither turbulent nor Hele-Shaw. Mostly, it is almost steady accompanied by large twin vortices behind the tube.

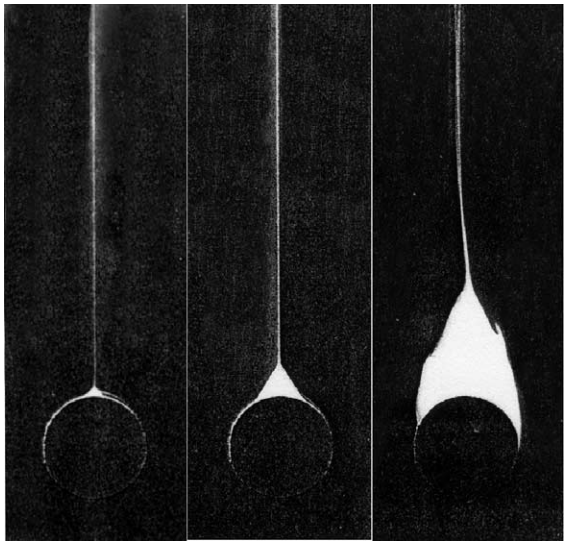

Fig. 1. Evolution of flow field behind the tube with increasing Reynolds number for $\delta/D = 0.06$, (a) $Re_D = 114$, (b) $Re_D = 425$, (c) $Re_D = 1270$.

This flow pattern is also well described by Tsai and Sheu [4] for $Re_D \leqslant 1000$ and $\delta/D = 0.19$. Note that the microscopic flow field ahead of the tube is not well visualized. Naphthalene sublimation experiment to be explained next will further reveal other aspects.

3. Experimental method using naphthalene sublimation technique

3.1. Test section

Fig. 2 is a schematic of the test section. The naphthalene plate is $130 \times 130 \times 10(t)$ mm^3, and made of

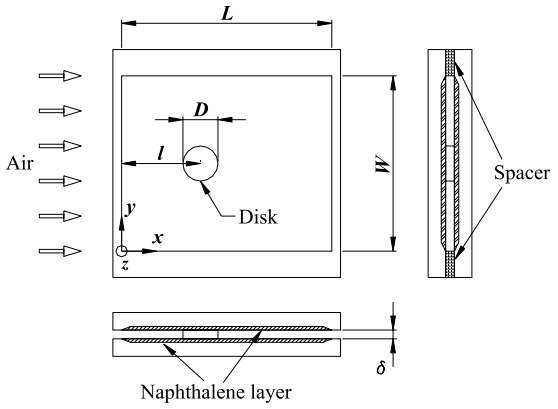

Fig. 2. Schematic of the test section.

stainless steel. The surface is polished and naphthalene is molded into a cavity. The molded naphthalene size is $100(W) \times 120(L) \times 2(t)$ mm^3. The circular Plexiglas disk to simulate the tube is 20 mm in diameter. It thus corresponds to a heat transfer problem where the fin efficiency is 100% while the heat transfer from the tube is not very important. The gap size (δ) is controlled by the thickness of the spacer made of Teflon and placed between the plates. The examined gap sizes are 4 and 6 mm. Actually, the flow at the inlet of test section is forward-facing step flow. However comparing the results of numerical simulations of two inlet conditions, forward-facing step flow and uniform flow, difference between the two cases almost disappears in the region behind 5 mm from the entrance where the naphthalene layer starts. Therefore, the inlet flow can be treated as uniform flow. And there are negligible effects of the spacer on the overall flow except nearby the spacer itself where wall effects in the order of the gap size δ are found to be evident (the numerical results are not shown here due to space limitation). In the experiments, the test section is completely sealed and immersed in water bath. The water in the bath is vigorously agitated and it is connected to a constant temperature water circulator to maintain uniform temperature.

3.2. Apparatus

Fig. 3 shows a schematic diagram of the experimental apparatus. This apparatus consists of two parts, one is for measurement and control of the volume flow rate of air and the other is for control of the water temperature. Dry air is supplied from an air bomb through two pressure regulators. Room air is not used to avoid hydration effect. The volume flow rate of air is measured with micro-manometer (max. 200 Pa) by measuring the pressure drop across a laminar-flow meter. This flow meter is made using 12 tubes of 4 mm inner diameter and 500 mm long. Airflow inside the tubes is perfectly laminar so that the theoretical Hagen–Poiseuille flow rate is almost identical with actual calibration using a bubble meter.

The vapor pressure of naphthalene is very sensitive to temperature. Pure naphthalene shows sublimation vapor pressure as [8]

$$T \log P = 0.5a_0 + \sum_{s=1}^{3} a_s E_s(x), \tag{1}$$

where

$$\begin{aligned} &a_0 = 301.6247, a_1 = 791.4937,\\ &a_2 = -8.2536, a_3 = 0.4043,\\ &x = (2T - 574)/114,\\ &E_1(x) = x, E_2(x) = 2x^2 - 1, E_3(x) = 4x^3 - 3x,\\ &P \text{ in Pa} \quad \text{and } T \text{ in K}. \end{aligned} \tag{2}$$

At room temperature, it varies about 10% per °C. Therefore the test section temperature is accurately maintained within 30 ± 0.1 °C by using the aforementioned water bath and circulator.

The schematic diagram of the sublimated naphthalene depth measurement system is shown in Fig. 4. It

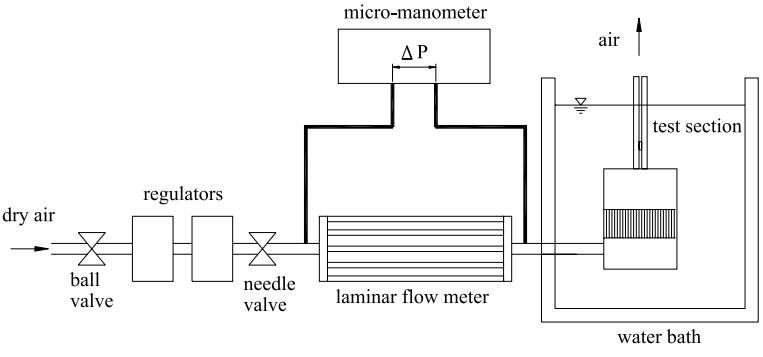

Fig. 3. Schematic diagram of the experimental apparatus.

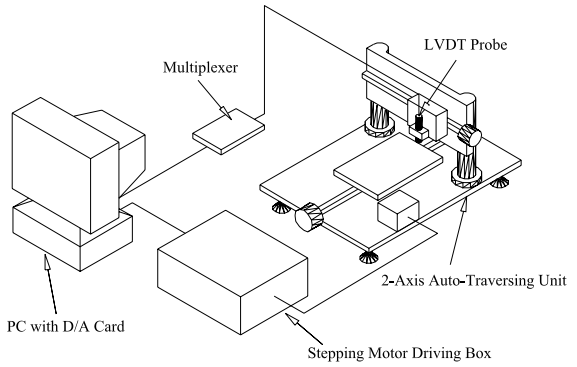

Fig. 4. Schematic diagram of the sublimated depth measurement system.

consists of a two-axis auto-traverse system, a depth gauge (LVDT) along with a data acquisition card and a personal computer for data storage and reduction. The two-axis auto-traverse system has step motors with a resolution of 1.8° per step (0.02 mm in linear direction). The depth gauge has range ±0.508 mm and linearity error of 0.170%. The total resolution of the LVDT and the analog-to-digital card is 0.25 μm and the sublimation depth uncertainty of the entire measurement system is 2 μm.

3.3. Procedure

Reagent grade (99% pure) naphthalene crystals are melted in a clean Pyrex glass beaker on a hot plate. The test section and the cover mold are cleaned with ethyl alcohol and pre-heated to prevent rapid solidification and subsequent clogging while pouring the molten naphthalene. The pouring speed and the naphthalene temperature are carefully controlled also. The cast plates are then separated from the cover mold by gentle hammering from the side to apply shear stress.

Before blowing air over the naphthalene plates, they are scanned by the depth measurement system. The scanning area is $100(x) \times 60(y)$ mm^2 and scanned points are 1 mm apart in both of the longitudinal and transverse directions. The total scanning time is about 1 h.

Then the plates are assembled and the whole assembly is immersed in the water bath, and the air flows over the naphthalene plates. The total blowing time is varied from 90 to 150 min depending on the rate of volume flow and the sublimation depth. Long blowing time gives greater sublimation depth. It thus improves the relative accuracy of the sublimation depth measurement. However, excessively long time changes δ significantly. In this experiment, the maximum distortion of geometry ($\mathrm{d}\delta/\delta$) is 0.038.

The local naphthalene sublimation depth is calculated from the local change of two surface elevation of before and after blowing. Difference in the mounting forces on the depth measuring system before and after blowing causes different overall warping of the plate. Thus, a reference surface is generated to compensate the warping. It is formed by measuring the elevation of eight points on the plate and smoothly connecting them.

3.4. Data processing

The local mass flux $\dot{m}''$ at each location is calculated from the following expression:

$$\dot{m}''(x,y) = \rho_s \frac{\tau(x,y)}{\Delta t}, \tag{3}$$

where ρ_s is the density of solid naphthalene, τ is the local sublimation depth, and Δt is the blowing time. The thermophysical properties of naphthalene, as well as the saturation vapor pressure, are obtained from Goldstein and Cho [8]. The local mass transfer coefficient h_m can then be calculated as follows:

$$h_m(x,y) = \frac{\dot{m}''(x,y)}{\rho_{sat} - \rho_{bulk}(x)}, \tag{4}$$

where ρ_{sat} is the saturation vapor density of naphthalene and represents the density of naphthalene vapor at the wall, and ρ_{bulk} is the bulk density of naphthalene vapor in the local airflow passing through the cross-section $x = \text{const}$. The saturation vapor density can be evaluated from the saturation vapor pressure and the perfect gas law, and the bulk density can be evaluated as

$$\rho_{bulk}(x) = \rho_{bulk}(0) + \frac{\dot{M}(x)}{\dot{Q}}, \tag{5}$$

where $\dot{Q}$ is the volume flow rate passing through the test section and $\dot{M}$ is the rate of mass transfer from both of the plates between 0 to x in x-direction and 0 to W (span) in y-direction. Since $\rho_{bulk}(0) = 0$ and $\dot{M}$ at x is given by (note that we have two naphthalene surfaces, up and down),

$$\dot{M}(x) = 2\int_0^x \int_0^W \dot{m}''(x,y)\,\mathrm{d}y\,\mathrm{d}x, \tag{6}$$

the local mass transfer coefficient h_m is finally expressed as

$$h_m(x,y) = \frac{\dot{m}''(x,y)}{\rho_{sat} - \frac{2}{\dot{Q}}\int_0^x \int_0^W \dot{m}''(x,y)\,\mathrm{d}y\,\mathrm{d}x}. \tag{7}$$

The local Sherwood number Sh_D based on tube diameter D is then calculated by

$$Sh_D = \frac{h_m D}{D_N}, \tag{8}$$

where D_N is the binary diffusion coefficient for naphthalene vapor in air. In this study, both local and span-

averaged results are compared. Span-averaging is performed as a simple arithmetic mean of the central 31 data points at 1 mm interval in y-direction.

3.5. Uncertainty analysis

Neglecting the measurement error of D in Eq. (8), the uncertainty in the local Sherwood number can be evaluated from,

$$(\mathrm{d}Sh_D)^2 = \left(\frac{\partial Sh_D}{\partial D_\mathrm{N}}\mathrm{d}D_\mathrm{N}\right)^2 + \left(\frac{\partial Sh_D}{\partial h_\mathrm{m}}\mathrm{d}h_\mathrm{m}\right)^2. \tag{9}$$

Or using Eq. (8),

$$\left(\frac{\mathrm{d}Sh_D}{Sh_D}\right)^2 = \left(\frac{\mathrm{d}D_\mathrm{N}}{D_\mathrm{N}}\right)^2 + \left(\frac{\mathrm{d}h_\mathrm{m}}{h_\mathrm{m}}\right)^2. \tag{10}$$

In this experiment, the uncertainty in diffusion coefficient D_N is 4.1%. Considering the complicated expression of h_m in Eq. (7), the uncertainty $\mathrm{d}h_\mathrm{m}$ can be expressed as,

$$(\mathrm{d}h_\mathrm{m})^2 = \left(\frac{\partial h_\mathrm{m}}{\partial \tau}\mathrm{d}\tau\right)^2 + \left(\frac{\partial h_\mathrm{m}}{\partial \dot{Q}}\mathrm{d}\dot{Q}\right)^2 + \left(\frac{\partial h_\mathrm{m}}{\partial \rho_\mathrm{sat}}\mathrm{d}\rho_\mathrm{sat}\right)^2 + \left(\frac{\partial h_\mathrm{m}}{\partial \rho_\mathrm{s}}\mathrm{d}\rho_\mathrm{s}\right)^2, \tag{11}$$

or

$$\left(\frac{\mathrm{d}h_\mathrm{m}}{h_\mathrm{m}}\right)^2 = \left(\frac{\mathrm{d}\tau}{\tau}\right)^2 + \left(\frac{\rho_\mathrm{bulk}}{\rho_\mathrm{sat}-\rho_\mathrm{bulk}}\frac{\mathrm{d}\dot{Q}}{\dot{Q}}\right)^2 + \left(\frac{\rho_\mathrm{sat}}{\rho_\mathrm{sat}-\rho_\mathrm{bulk}}\frac{\mathrm{d}\rho_\mathrm{sat}}{\rho_\mathrm{sat}}\right)^2 + \left(\frac{\rho_\mathrm{bulk}}{\rho_\mathrm{sat}-\rho_\mathrm{bulk}}\frac{\mathrm{d}\rho_\mathrm{s}}{\rho_\mathrm{s}}\right)^2. \tag{12}$$

In the far downstream region, the above uncertainty reaches a maximum since ρ_bulk approaches ρ_sat indefinitely. By using the data of that region, the uncertainties in τ, $\dot{Q}$, ρ_sat and ρ_s are 4%, 4.5%, 3.9% and 1.1%, respectively. The magnification factors $\rho_\mathrm{bulk}/(\rho_\mathrm{sat}-\rho_\mathrm{bulk})$ and $\rho_\mathrm{sat}/(\rho_\mathrm{sat}-\rho_\mathrm{bulk})$ are then 0.77 and 1.77, respectively. Comprising all these uncertainties, the net uncertainty in Sh_D is found to be 9.7%.

4. Results and discussion

The following parameters are taken in the experiments. The span to diameter ratio W/D is fixed to 5.0 and the length to span ratio L/W is fixed to 1.2. For the varied parameters, δ/D is taken as 0.2 and 0.3, Re_D is taken as 950 and 2660 for $\delta/D = 0.2$ and 1770 for $\delta/D = 0.3$, and finally l/D is extensively varied as 0.75, 1.0, 1.5, 2.5 and 3.5. These are taken to be as much realistic as possible, and they give a reasonable air-side effectiveness of around 0.2 to 0.6.

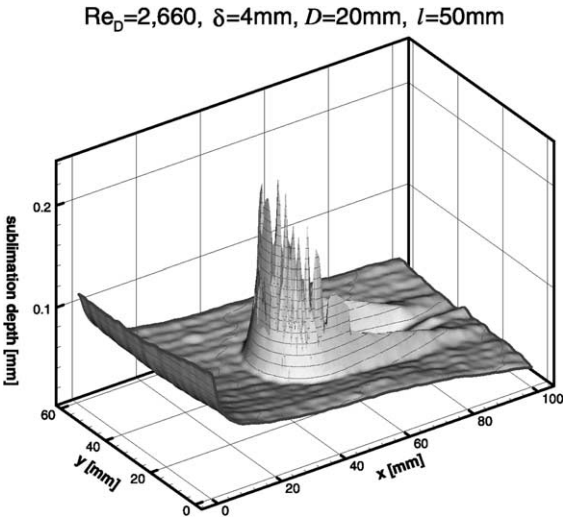

Fig. 5. A typical 3-D plot of the sublimation depth.

First of all, a qualitative evaluation of the microscopic phenomena is provided. Fig. 5 shows a three-dimensional plot of sublimation depth with $Re_D = 2660$ (corresponding to $U = 2.1$ m/s), $l/D = 2.5$ and $\delta/D = 0.2$. It is obtained after 90 min of air blowing. It is large at the leading edge of the plate and also in front of the tube. It is relatively small behind the tube and it decreases asymptotically to the fully developed value far downstream.

The high mass transfer rate at the leading edge is due to the thin boundary layer beginning to develop. It is almost identical with the case of a flat plate in infinite stream. The mass transfer rate decreases rapidly along the downstream. The local Sherwood number approaches asymptotically to the fully developed value (7.54 times $D/2\delta$) in the far downstream. The entrance or developing length is greater for greater air velocity and gap size. Greater entrance length means thinner boundary layer on the fin resulting in the increase in the total heat transfer rate, as also has been depicted by Romero-Mendez et al. [7].

When the boundary layer is developed fully in the gap, the mass transfer coefficient becomes a constant while the bulk flow is being saturated with naphthalene vapor. Consequently, the mass transfer rate in the downstream is further reduced, approaching zero eventually.

Flow around the tube is typified by the existence of trailing twin vortices and a leading horseshoe vortex. The former is very detrimental to mass transfer. Air velocity is very low in the recirculating twin vortices and it is almost saturated with naphthalene vapor. The mass transfer rate thus becomes very small, and for this

reason, Onishi et al. [5] assert that the recirculating twin vortices region behind the tube may well be eliminated for more efficient heat transfer.

Saboya and Sparrow [1] clearly show that a horseshoe vortex exists ahead of the tube and it is larger for larger Reynolds number. In their experiments, Re_D is from 496 to 2950 based on the tube diameter. The experimental results of this research confirm their finding: there exists a horseshoe vortex in front of the tube rotating in a clockwise direction above the bottom side plate in the x–z plane. It wraps around the tube and extends its trail along the side of the tube. The upper plate has a mirror-image horseshoe vortex rotating in the opposite direction. Its existence is clearly marked by a deep U-shaped groove around the tube, shown in Fig. 5 as the high wall ahead and beside the tube. Though not shown here due to limited space, the mass transfer coefficient along the frontal line of the groove is very small since the flow is separated there.

When Re_D is as large as 2660 for $\delta/D = 0.2$, another small horseshoe vortex appears ahead of the main horseshoe vortex, in contrast to the only appreciable main one for $Re_D = 950$. Though the overall size is small, it leaves a smaller groove ahead of the main groove. Saboya and Sparrow's experiments [1] also show a clear evidence of the subsidiary horseshoe vortex for $Re_D = 2950$. Fig. 6 gives an illustration of the two pairs of horseshoe vortices for better understanding.

The span-averaged local Sh_D with various locations of the tube is shown in Fig. 7. The Sherwood number is greatest at the leading edge of the plate and then in front of the tube as shown previously. The effect of the location of the tube is clearly shown in this figure. As the tube is placed in the downstream region, the positive effect of the horseshoe vortex on mass transfer rate is prominent and the negative effect of the recirculating twin vortices behind the tube is diminished. Therefore, it is better to place the tube in downstream position for

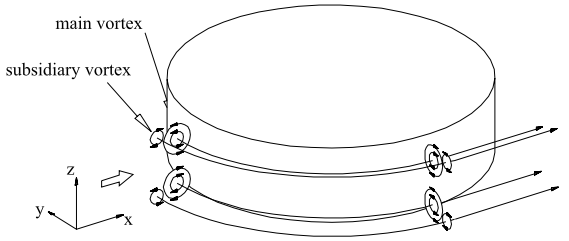

Fig. 6. Illustration of the main and the subsidiary horseshoe vortices around the tube.

enhanced heat transfer. Another evaluation of this judgment comes from the fact that magnitude of the local mass transfer coefficient around the horseshoe vortex is almost independent of the tube location. When the tube is located close to the leading edge the mass transfer coefficient in front of the tube is not increased appreciably since it is already very high there. To the contrary, placing the tube in the downstream region greatly increases the total mass transfer rate. Fig. 8 concisely shows the effect of the positioning of the tube. Proper positioning of the tube in the view point of heat/mass transfer is estimated to increase the total mass transfer rate by about 25%, compared with the case of $l/D = 0.75$ for any δ/D and Re_D.

With respect to Re_D, 180% increase of Re_D causes 85% increase in the total mass transfer rate (compare the two cases of $\delta = 4$ mm with $\dot{Q} = 850$ cm^3/s and 300 cm^3/s in Fig. 8). If the total mass transfer rate is proportional to Re_D, then the proper positioning is equivalent to about 50% increase of Re_D. As can be seen from Fig. 8 also, the total mass transfer rate is decreased by 10% by 50% increase of the gap size at a fixed airflow rate of 850 cm^3/s (compare the two cases of $\dot{Q} =$ 850 cm^3/s with $\delta = 4$ and 6 mm). It should not be confused, however, that increase of airflow rate pro-

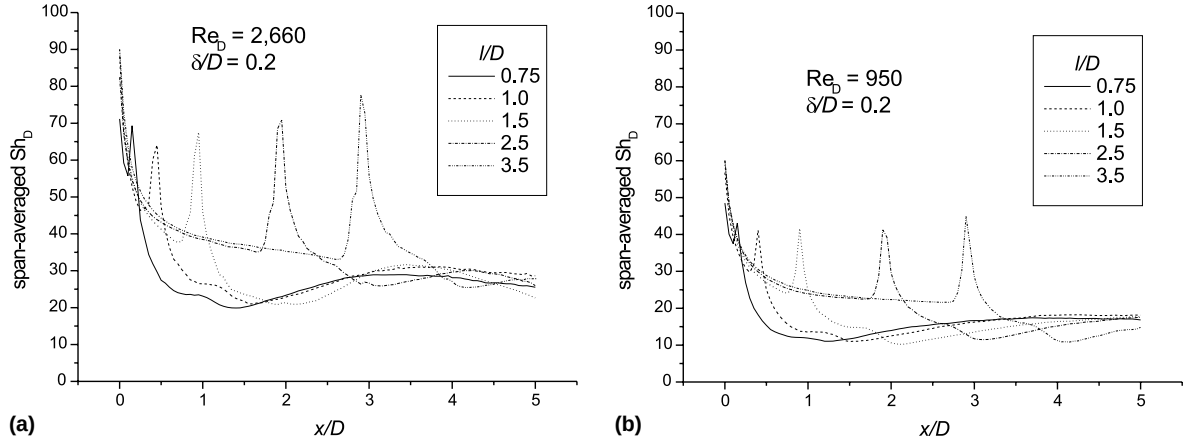

Fig. 7. Span-averaged Sh_D along the longitudinal direction with various tube positioning, (a) $Re_D = 2660$, (b) $Re_D = 950$.

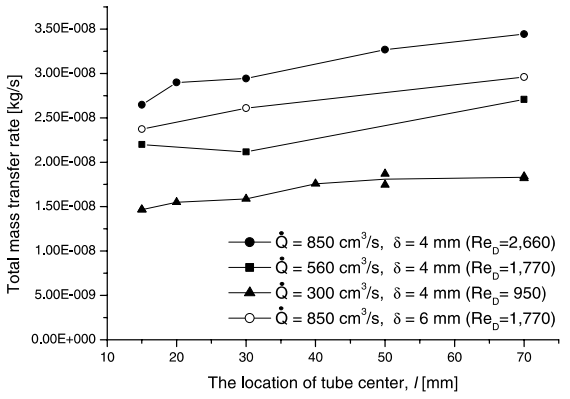

Fig. 8. Effect of the location of tube center ($D = 20$ mm) on total mass transfer rate with various Re_D and gap size.

portional to the gap size (thus maintaining the same air velocity in two cases of $Re_D = 1770$ with $\delta = 4$ and 6 mm) increases the total mass transfer rate also [7].

Fig. 9 shows the existence of the subsidiary horseshoe vortex through the secondary peaks of the curves. Though the results are not shown here, the size of the horseshoe vortex is increased with the gap size at the same airflow rate. However at the same time, the strength of vortex is reduced, so the total mass transfer rate is decreased.

The final inquiry is about the pressure drop. Fig. 10 shows the friction factor f defined from

$$\Delta p = f \frac{\rho_{\text{air}} v^2}{2} \frac{L}{\delta}, \tag{13}$$

where Δp is the total pressure drop from $x = 0$ to L. As can be found from the graph, the friction factor with disk is greater than that without disk. Also, the friction factor is roughly inversely proportional to Re_D. However, it is noteworthy that it is almost insensitive to the

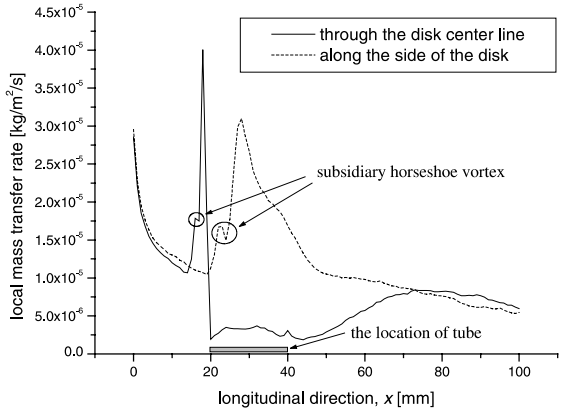

Fig. 9. Local mass transfer rate along the longitudinal direction, when $\dot{Q} = 850$ cm^3/s, $\delta = 4$ mm ($Re_D = 2660$).

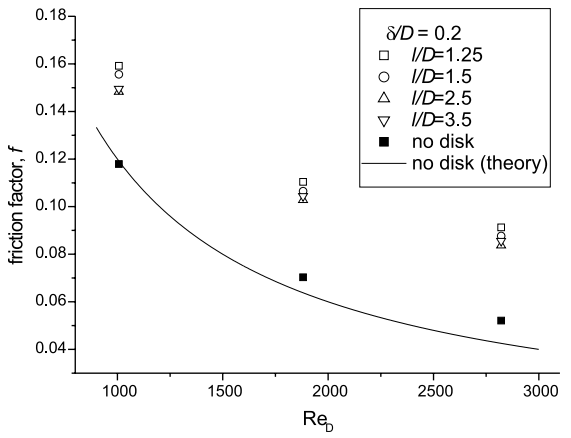

Fig. 10. Effect of the location of tube center on friction factor with various Re_D.

disk location. Consequently, all the earlier discussion on heat transfer augmentation by relocating the disk center is perfectly valid without any further penalty of increased pressure drops.

5. Conclusion

To investigate the microscopic flow and heat transfer phenomena and also to evaluate the overall performance to find out the optimal tube location, the local mass transfer coefficient on the plate is calculated from the measurement of sublimated naphthalene depth. The examined parameters are the gap to tube diameter ratio δ/D, the Reynolds number Re_D and the tube location l/D.

The local mass transfer rate is large at the leading edge of the plate and also in front of the tube in all examined cases. The horseshoe vortex formed in front of the tube gives significant increase in the total heat/mass transfer rate.

The subsidiary horseshoe vortex is formed when Re_D is increased to as high as about 2660 for $\delta/D = 0.2$.

Mass transfer is very inactive in the recirculating twin vortex and in the far downstream.

The tube is better placed at downstream to increase the total heat/mass transfer rate at any δ/D and Re_D. Proper positioning of the tube is estimated to increase the total mass transfer rate up to 25%. Further researches on multiple tube interaction are recommended.

Acknowledgements

This work has been supported by the Critical Technology 21 Project of the Ministry of Science and Technology, Korea.

References

[1] F.E.M. Saboya, E.M. Sparrow, Local and average transfer coefficients for one-row plate fin and tube heat exchanger configurations, ASME J. Heat Transfer 96 (1974) 265–272.

[2] F.E.M. Saboya, E.M. Sparrow, Transfer characteristics of two-row plate fin and tube heat exchanger configurations, Int. J. Heat Mass Transfer 19 (1976) 41–49.

[3] J.Y. Jang, M.C. Wu, W.J. Chang, Numerical and experimental studies of three-dimensional plate-fin and tube heat exchangers, Int. J. Heat Mass Transfer 39 (14) (1996) 3057–3066.

[4] S.F. Tsai, T.W.H. Sheu, Some physical insights into a two-row finned-tube heat transfer, Comput. Fluids 27 (1) (1998) 29–46.

[5] H. Onishi, K. Inaoka, K. Matsubara, K. Suzuki, Heat transfer performance of a plate-finned tube heat exchanger (a three-dimensional steady numerical analysis for a single row tube), in: Proceedings of the Eleventh International Heat Transfer Conference, Kyongju, vol. 6, 1998, pp. 227–232.

[6] H. Onishi, K. Inaoka, K. Matsubara, K. Suzuki, Numerical analysis of flow and conjugate heat transfer of a two-row plate-finned tube heat exchanger, in: Proceedings of the Second International Conference on Compact Heat Exchangers and Enhancement Technology for the Process Industries, Banff, 1999, pp. 175–182.

[7] R. Romero-Mendez, M. Sen, K.T. Yang, R. McClain, Effect of fin spacing on convection in a plate fin and tube heat exchanger, Int. J. Heat Mass Transfer 43 (2000) 39–51.

[8] R.J. Goldstein, H.H. Cho, A review of mass transfer measurements using naphthalene sublimation, Exp. Thermal Fluid Sci. 10 (1995) 416–434.